

Computational and experimental analysis of granular flow in hoppers

Devang Khakhar^{1,*}, Jeetram Yogi¹, and Afroz Momin¹

¹Department of Chemical Engineering, Indian Institute of Technology Bombay, Powai, Mumbai 400076, India

Abstract. Hoppers are among the most widely used equipment for granular material processing in industry. We present experimental and DEM simulation results for the flow of granular material in wedge-shaped hoppers. The predictions of theory of Savage for a wedge-shaped hopper with frictionless walls and a theory using the μ - I rheology, are compared to DEM simulation results. The μ - I rheology gives a very good match to the simulation results. The velocity field in a quasi-2D wedge-shaped hopper, with front and back match walls, is obtained experimentally using image analysis and particle tracking. We find that the radial velocity in cylindrical coordinates varies as $v_r \propto \theta^2$, and that the tangential velocity is non-zero, but much smaller than the radial velocity. The experimental velocity distributions closely match the DEM simulation results using calibrated parameters. DEM simulations without the front and back walls yield qualitatively similar results to the quasi-2D case. Analysis of the flow in the exit region indicates that velocity varies smoothly over the domain and a *free fall arch* is not evident. The vertical acceleration data indicate that the particles experience free fall only a significant distance below the exit plane. The acceleration is larger than the acceleration due to gravity near the exit, which is explained in terms of an arch-buckling mechanism.

1 Introduction

Bins and hoppers are among the most widely used equipment in industrial granular processes [1, 2]. They are used for storage of raw materials and products and for continuous feeding of materials. Our focus is on the latter for freely flowing particles. Bins have a flat bottom with an orifice in the centre for feed of materials, while hoppers have a conical lower section. In both systems there is a converging flow of the granular material. In the bin the converging zone is determined by the particles forming a fixed bed in the corners of the bin, while in the hopper, for small cone angles, there is no stagnant zone and the converging flow is determined by the cone angle. More complex behaviour is exhibited by cohesive particles, including rat-holing, channeling, etc. [2], but we consider only freely flowing particles here.

Given its practical importance, the flow in bins and hoppers has been widely studied starting with the work of Brown and Richards [3]. An important early result was the empirical equation for the mass flow rate by Beverloo *et al.* [4] who found that the mass flow rate from hoppers was proportional to $(D_o - \alpha d_p)^{5/2}$, independent of the height of filling in the hopper, and also independent of the other geometrical parameters. Here D_o is the orifice diameter, d_p is the particle diameter and $\alpha \approx 1.5$ is a constant. The Beverloo correlation [4] implies that the mass flow rate from the hopper is essentially determined by the local flow in the region of the exit, which has been studied in considerable detail in recent times [5–7], particularly in the context of the *free fall arch* theory [8]. The latter postulates that par-

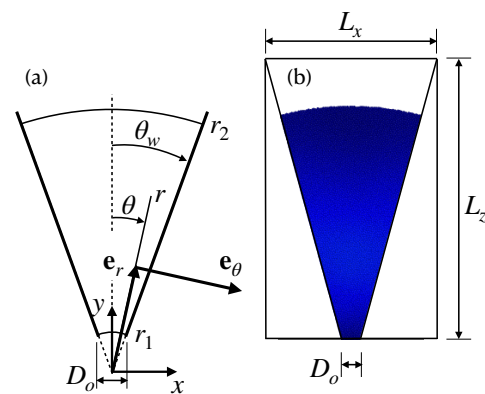


Figure 1. (a) Schematic view of a wedge-shaped hopper showing the coordinate system and geometrical dimensions. The unit vectors for the cylindrical coordinate system used (\mathbf{e}_r , \mathbf{e}_θ) are also shown. (b) Snapshot of system used in the simulation studies.

ticles form an arched surface at the exit, blocking the flow. Below the arched surface particles fall freely under gravity. As a consequence of the formation of the arched surface, the velocity and acceleration are expected to change sharply across the surface. Such arch formation has not been observed in previous studies [5].

Experimental studies of the velocity field by Nedderman [9] and Cleaver and Nedderman [10] showed that the flow in 3D conical hoppers is purely radial, $\mathbf{v} = (v_r, 0, 0)$, in spherical coordinates, with $v_r = f(\theta)/r^2$. The function $f(\theta)$ is maximum at the centerline of the hopper. Similar studies in a 2D wedge-shaped hopper also found the ve-

*e-mail: khakhar@iitb.ac.in

locity field to be purely radial in cylindrical coordinates (see Fig. 1a), with the time averaged radial velocity given by $v_r = f(\theta)/r$ [11]. The measurements indicated large velocity fluctuations due to local jamming, resulting from the converging flow of the rigid particles.

Jenike [12] developed a theory for the stress distribution for flowing material in a wedge-shaped hopper assuming that material is purely frictional and that an analogue of the Mohr-Coulomb yield condition (the Shield-Jenike equation) is satisfied at each point in the flowing material [13]. The Shield-Jenike equation was validated by Jenike [13] through extensive experimentation. The velocity in the system is indeterminate since the stresses in the constitutive relation are independent of the shear rate. Savage [14] considered a simplified hopper system with frictionless walls and radially directed gravity to obtain a closed form solution for the velocity and stress fields. The velocity was determined by including the inertial terms in the momentum balance equation. Brennen and Pearce [15] presented a perturbation solution using the same assumptions as Savage [14] but including wall friction. They showed that the velocity field in the hopper, in the limit of low wall friction, is of the form

$$v_r = v_{r0}(r) + \varepsilon^2 v_{r2}(r) (\theta/\theta_w)^2 \quad (1)$$

$$v_\theta = \varepsilon^3 v_{\theta3}(r) (\theta/\theta_w)^3 \quad (2)$$

where ε is a small parameter and θ_w is the wedge-angle of the hopper (Fig. 1a).

In this paper we present results for the flow in a wedge-shaped hopper based on experiments in a quasi-2D system with front and back glass walls and Discrete Element Method (DEM) simulations for an identical system. DEM simulation results are also presented for systems in which the front and back walls are replaced by periodic boundaries. The objective is to highlight some of the important features of the flow in the system. In the next section, we discuss the Savage [14] model and a model based on the μ - I rheology [16] for flow in a wedge-shaped hopper with frictionless sidewalls. Predictions of both models are compared to results of DEM simulations. Experimental measurements of the velocity field in a quasi-2D system and comparison to DEM simulation results are presented next. Experimental measurements of the flow in the exit region along with DEM simulation results are presented in section 4. Conclusions of the paper are given in the final section.

2 Wedge-shaped hopper with frictionless walls

We present here the model of Savage [14] and a model for the flow based on the μ - I rheology. Predictions of both models are compared to DEM simulation results. The work presented here is a review of the results in Ref. [17].

Savage [14] considered a wedge-shaped hopper with frictionless walls and radial gravity, shown schematically in Fig. 1a. The cylindrical coordinate system used in the analysis is also defined in the figure. With the above assumptions, none of the variables depend on θ and the shear

stress ($\sigma_{r\theta}$) and tangential velocity (v_θ) are zero. In this case, the radial velocity from the continuity equation is obtained as

$$v_r = -A/r, \quad (3)$$

where A is a constant. Since $\sigma_{r\theta} = 0$, the normal stresses ($\sigma_{rr}, \sigma_{\theta\theta}$) are principal stresses, and the Shield-Jenike equation [13] gives

$$\frac{\sigma_{\theta\theta}}{\sigma_{rr}} = k = \frac{1 + \sin\beta_s}{1 - \sin\beta_s}, \quad (4)$$

where k is a constant and β_s is the angle of internal friction. The value of the stress ratio, k , in the flowing material is found to be larger than that at the Mohr-Coulomb yield point [13].

The steady state r -component of the stress balance equation, using Eqs. (3) and (4), reduces to

$$\frac{d\sigma_{rr}}{dr} - (k-1) \frac{\sigma_{rr}}{r} = -\rho g + \frac{\rho A^2}{r^3}, \quad (5)$$

where ρ is the bulk density. The second term on the right hand side ($\rho A^2/r^3$) is due to inertia and depends on the velocity. The above equation is easily integrated to obtain σ_{rr} with two unknown constants: the constant of integration and A . Savage used the boundary conditions, $\sigma_{rr} = 0$ at $r = r_2$ (free surface) and $\sigma_{rr} = 0$ at $r = r_1$ (exit), to obtain expressions for the velocity (v_r) and stress (σ_{rr}).

The μ - I rheology [16] can be substituted for the Shield-Jenike-equation [13], by noting that

$$\frac{\sigma_{\theta\theta}}{\sigma_{rr}} = \frac{1 + \mu(I)}{1 - \mu(I)} = k_d(I), \quad (6)$$

for the μ - I rheology, where

$$\mu = (\sigma_{\theta\theta} - \sigma_{rr})/(\sigma_{\theta\theta} + \sigma_{rr}) \quad (7)$$

is effective coefficient of friction, and

$$I = \dot{\gamma} d_p (\rho_p/P)^{1/2} \quad (8)$$

is the inertial number with the pressure, $P = (\sigma_{\theta\theta} + \sigma_{rr})/2$, and shear rate, $\dot{\gamma} = 2A/r^2$. The stress balance equation in this case is the same as Eq. (5), but with k replaced by $k_d(I)$. The equation becomes non-linear with this substitution, and a numerical integration is required.

DEM simulations are carried out to precisely replicate the geometry used in the Savage [14] model (Fig. 1b). We present results here for a wedge angle, $\theta_w = 15$ deg., and a thickness of the hopper normal to the plane of flow, $b = 1$ cm, which periodic boundary conditions in this direction. The side walls of the hopper are flat frictionless surfaces. The hopper is first filled with the exit closed, and next the top surface is shaped by removing all particles with $r > r_2$. This state is shown in Fig. 1b. The exit is opened next and the flow accelerates from rest. Data is collected after an interval of flow, when the flow has achieved a steady state. The duration of the flow from the hopper when the data is collected is short, so that the change in height, r_2 , during data collection is small. Averaging is done for a large number (30) of such fill-cut-flow cycles. Simulations are

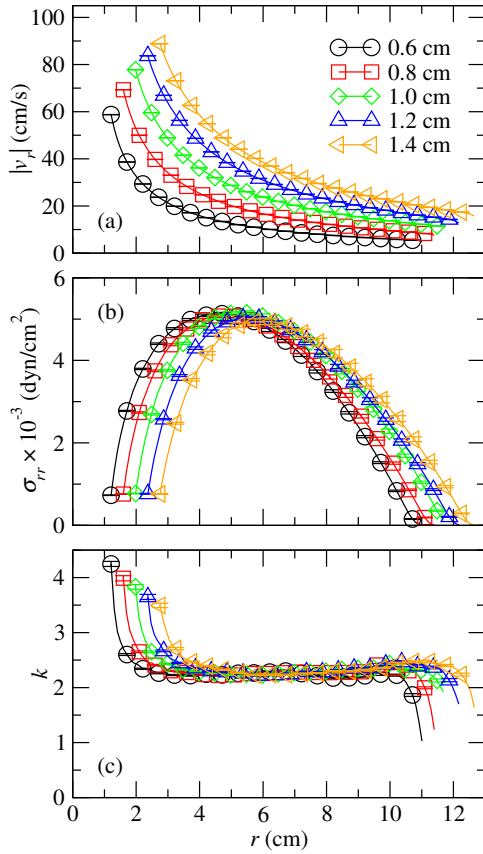


Figure 2. DEM simulation results for a hopper with frictionless walls showing the variation of (a) the velocity ($|v_r|$), (b) stress (σ_{rr}) and (c) stress ratio (k) with radial distance (r) for different orifice widths (D_o) given in the legend. ($1 \text{ dyn/cm}^2 = 0.1 \text{ Pa}$)

carried out using LAMMPS [18] with interparticle forces computed using a spring-dashpot model and the friction implemented by a history dependent contact in which the relative tangential displacement is normalized so that the ratio of the tangential to normal force at a contact is not greater than the friction coefficient, μ_p . The particle properties used are: particle diameter, $d_p = 0.1 \text{ cm}$, with a polydispersity in diameter of 10% to prevent crystallization, particle density, $\rho_p = 2.5 \text{ g/cm}^3$, coefficient of restitution, $e = 0.88$, particle stiffness, $k_n = 2.568 \times 10^6 \text{ dyn/cm}$ and interparticle friction coefficient, $\mu_p = 0.5$.

Fig. 2 shows the variation of the velocity magnitude ($|v_r|$), stress (σ_{rr}) and stress ratio (k) with radial distance (r) for hoppers with different orifice widths, D_o . The velocity reduces with distance from the orifice (increasing r) and increases with increasing orifice width (Fig. 2a). The stress has a maximum of $\sigma_{rr, \text{max}} \approx 5000 \text{ dyn/cm}^2$ at an intermediate radial position, and the maximum stress is nearly independent of the orifice width, D_o (Fig. 2b). The finite (non-zero) stress at the exit is clearly apparent in the figure. The data for the stress ratio collapse to $k \approx 2.1$ for all the orifice widths over most of the hopper, excluding the exit region (Fig. 2c). This indicates that the Shield-Jenike equation is valid over most of the hopper, but does not apply near the exit where the shear rates are high. We thus consider the μ - I model to account for this deviation.

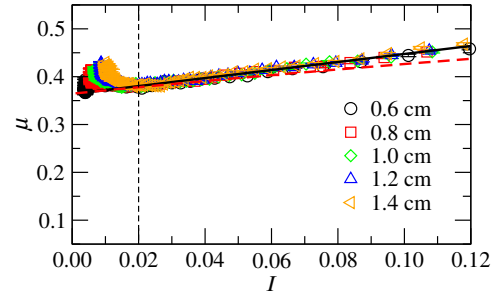


Figure 3. DEM simulation results for a hopper with frictionless walls showing the variation of the friction coefficient (μ) with the inertial number (I) for different orifice widths (D_o) given in the legend. The solid line is a fit of Eq. (9) and the dashed line is a fit to the data for a shear flow.

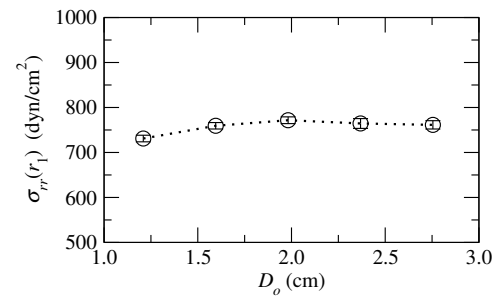


Figure 4. DEM simulation results for a hopper with frictionless walls showing the variation of the stress at the exit ($\sigma_{rr}(r_1)$) with orifice width (D_o).

The stress ratio (k) reduces near the free surface ($r \approx 12 \text{ cm}$, Fig. 2c), which implies that μ reduces near the free surface, in agreement with the results of Roy *et al.* [19].

The data for the friction coefficient (μ) versus the inertial number (I), computed from the simulation data using Eqs. (7) and (8) for the different orifice widths (D_o), are shown in Fig. 3. The data collapse to a straight line

$$\mu = \mu_s + aI, \quad (9)$$

except for data for $I < 0.02$. These data correspond to the region near the free surface, where the total deformation during flow is too small to achieve equilibrium. The first term in Eq. (9) corresponds to frictional stresses and the second to viscous stresses arising from interparticle collisions and streaming. When $a = 0$, the μ - I model reduces to the Shield-Jenike model. A least squares fit of Eq. (9) to the data for $I > 0.02$, shown as a black line in Fig. 3, yields $\mu_s = 0.365$ and $a = 0.827$. The variation of μ versus I for a shear flow of the identical particles is shown in Fig. 3 as a red dashed line. The shear flow and hopper flow results are slightly different implying that rheology for the converging flow is slightly different from that for a shear flow. A similar result was reported by Bhateja and Khakhar [20] for a rectangular hopper.

Simulation results given in Fig. 2b indicate that the stress at the exit, $\sigma_{rr}(r_1)$, is significant. The computed exit stresses for different orifice widths (D_o) are shown in Fig. 4. The magnitudes of the exit stresses are about 10-

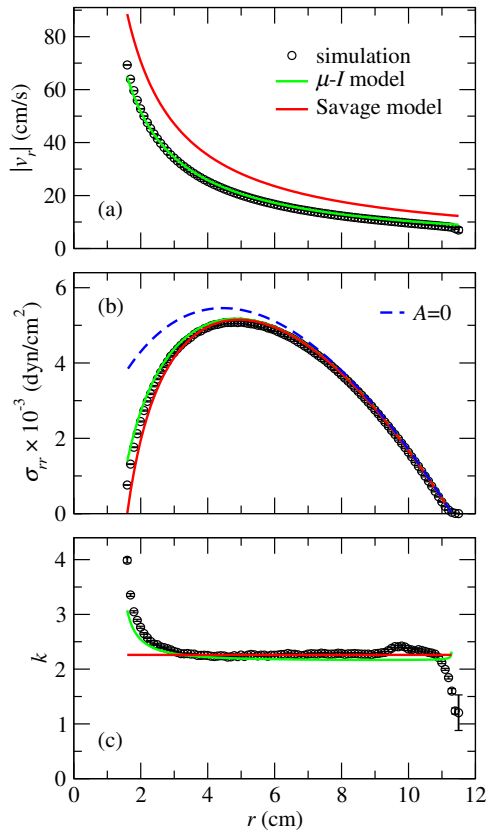


Figure 5. Comparison of the profiles predicted by the Savage [14] model and the μ -I model to DEM simulation results for the (a) velocity ($|v_r|$), (b) stress (σ_{rr}), and (c) stress ratio (k).

15% of the maximum stress in the system for the different cases studied. This is contrary to the assumption of zero stress at the exit ($\sigma_{rr}(r_1) = 0$) in the Savage [14] model.

A comparison of the predictions of the Savage [14] model and the μ -I based model to DEM simulation results is shown in Fig. 5. In the Savage [14] model A is obtained by using the boundary condition $\sigma_{rr}(r_1) = 0$, and the stress ratio, k , is obtained by fitting to DEM simulation results for k in the central region, where it is nearly constant. In the μ -I model, the parameters μ_s , a obtained above are used, and A is obtained by fitting Eq. (3) to the velocity data from the simulations. This is an alternative to using the exit stress boundary condition. The Savage [14] model predicts a significantly higher velocity (Fig. 5a), since the exit stress, which is a measure of the resistance to the flow out of the hopper, is not accounted for. Both models predict the stress variation very well, however, the Savage [14] model deviates in the exit region since it assumes a zero stress at the exit and neglects viscous stresses, which are significant at the exit (Fig. 5b). The μ -I model correctly predicts the increase in k_d at the exit due to viscous stresses, however, assuming a constant value of the stress ratio, k , is a reasonable approximation in the region away from the exit (Fig. 5c). The predictions of the μ -I model excluding inertia ($A = 0$ in Eq. (5)), are also shown in Fig. 5b. They exhibit a significant deviation from the sim-

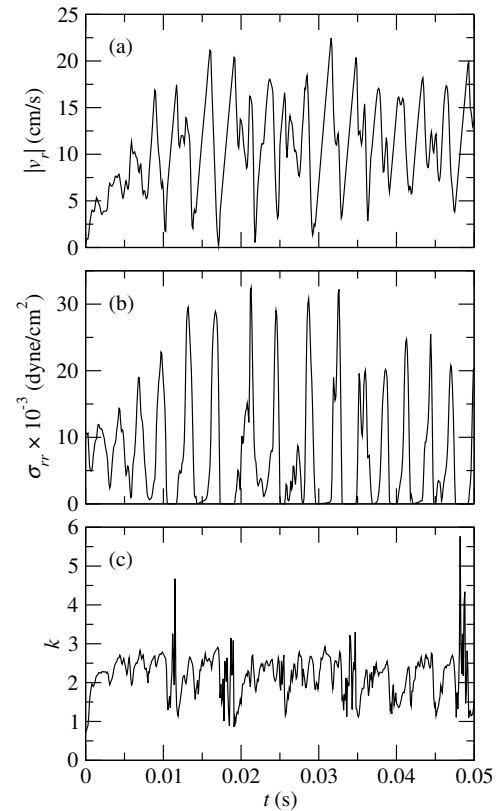


Figure 6. DEM simulation results for a hopper with frictionless walls showing the variation of (a) the velocity ($|v_r|$), (b) stress (σ_{rr}) and (c) stress ratio (k) with time (t) at $r = 12$ cm for an orifice width $D_o = 1$ cm and fill height $r_2 = 21$ cm.

ulation results, indicating that inertial effects are important in the flow.

Schaeffer [21] showed that the governing equations based on the Shield-Jenike rheology are unstable in the same sense as the energy balance equation with a negative thermal conductivity is. He conjectured that the instability was the cause of the large flow fluctuations observed in practical hopper flows. More recently, Barker *et al.* [22] showed that the μ -I rheology is also unstable in some regions of the parameter space. We observed large velocity and stress fluctuations in our simulations on short time scales, which may be an indicator of the instability. Similar large fluctuations were observed previously by Vivanco *et al.* [11]. Fig 6 shows the variation of the velocity (v_r), stress (σ_{rr}) and stress ratio (k) with time (t) for a typical case. For all three, the fluctuations are of the same order of magnitude as the mean values, with a frequency of about 250 Hz. Despite this, the time-averaged behaviour of the system is well described by theories based on the Shield-Jenike and the μ -I rheologies, as shown above (Fig. 5).

Fig. 7 shows the variation of the computed mass flow rate (\dot{m}) with the theoretical prediction ($\theta_w Ab$) using fitted values of A , for different orifice widths (D_o). The fitted straight line passes through the origin and shows a good agreement between the simulation results and predictions of the theory. Further, we find $A \propto (r_1 - \alpha d_p)^{3/2}$ with $\alpha = 1.6$. The mass flow rate, thus, follows the Bever-

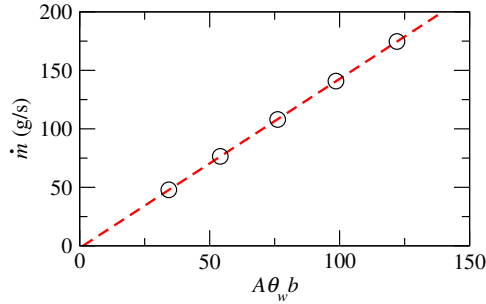


Figure 7. DEM simulation results for a hopper with frictionless walls showing the variation of the mass flow rate (\dot{m}) with the theoretical prediction ($A\theta_w b$) for fitted values of A for different orifice widths (D_o). The solid line is a fit to the data.

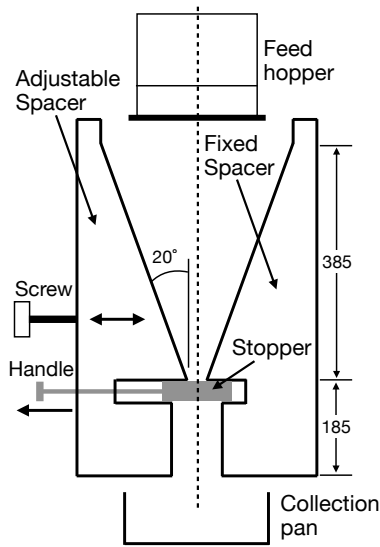


Figure 8. Schematic view of the wedge-shaped hopper used in experiments. The screw is used to adjust the horizontal position of the left spacer and thus control the orifice width, D_o . The handle is used to slide the stopper plate to block/unblock the orifice.

loo [4] correlation in 2D, and α is close to the reported experimental values. A detailed experimental study of the velocity field in the hopper is discussed in the next section.

3 Velocity field in a quasi-2D hopper

We measure the velocity field in a wedge-shaped hopper shown schematically Fig. 8. The hopper angle is $\theta_w = 20$ deg. and thickness is 1.2 cm, with glass front and back walls. Other dimensions of the apparatus are shown in the figure. A video recording is made of the flowing particles at the front glass wall, and the particle velocities are determined using image analysis and particle tracking. Data is presented here for glass beads of diameter $d_p = 1.86 \pm 0.17$ mm and different orifice widths, D_o . Each experiment is repeated 5 times and the mean values and standard errors are reported. DEM simulations for a geometrically identical system are also carried out. The objective is to carry out a detailed characterization of the velocity field using

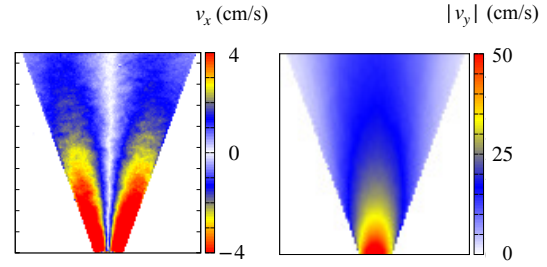


Figure 9. Experimentally measured spatial distribution of the horizontal velocity (v_x) and vertical velocity ($|v_y|$) in the quasi-2D hopper for an orifice width $D_o = 2.5$ cm for $d_p = 1.86$ mm glass particles.

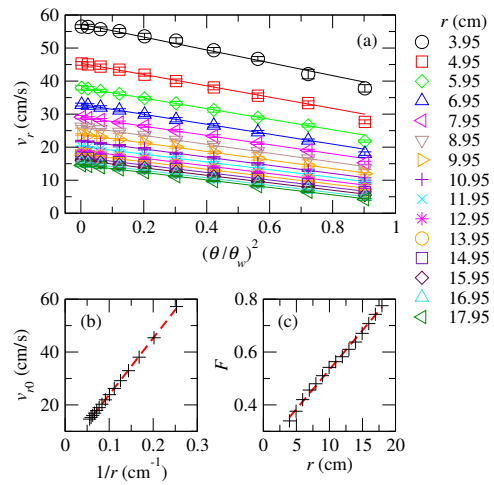


Figure 10. Variation of the experimentally measured radial velocity ($|v_r|$) with the square of the scaled angle $[(\theta/\theta_w)^2]$ at different radial positions, r (symbols), for 1.86 mm glass particles and an orifice width $D_o = 2.5$ cm. Error bars indicate the standard error. Lines are fits of Eq. (10) to the data. (b) Variation of the fitted centerline velocity (v_{r0}) with $1/r$, and (c) variation of the fitted values of the effective wall friction (F) with radius (r).

the theory of Brennen and Pearce [15] as a framework. The results presented here are a summary of a more detailed investigation given in Ref. [23].

Fig. 9 shows the spatial distribution of the horizontal (v_x) and vertical ($|v_y|$) velocity components in the hopper. The direction of horizontal velocity is inward toward the centerline of the hopper and the horizontal velocity at the centerline is zero, due to symmetry. The vertical velocity is downward and is also symmetric about the centerline. Both velocities decrease with distance from the exit. The magnitude of the horizontal velocity (v_x) is more than an order of magnitude smaller than the vertical velocity (v_y).

Fig. 10 shows the variation of the measured radial velocity ($|v_r|$) with the square of the scaled angle $[(\theta/\theta_w)^2]$ at different radial distances (symbols). The velocity varies linearly with $(\theta/\theta_w)^2$ as predicted by Brennen and Pearce [15], and decreases with increasing distance from the exit. The straight lines are fits of

$$v_r = v_{r0}(r) \left[1 - F(r) (\theta/\theta_w)^2 \right], \quad (10)$$

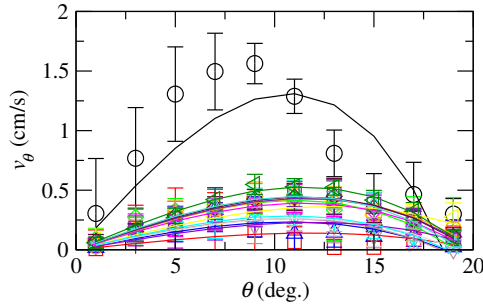


Figure 11. Comparison of the experimentally measured tangential velocity profiles ($v_\theta(\theta)$) (symbols) with predictions of v_θ obtained from the continuity equation using Eq. (10) (lines) for 1.86 mm glass particles with orifice width $D_o = 2.5$ at different radial positions, r , as given in the legend of Fig. 10. Error bars indicate the standard error.

and the fitted values of v_{r0} and F at each radial position are shown in Figs. 10b,c (symbols). v_{r0} is the centerline velocity ($v_r(r, 0)$) and $(1 - F) = v_r(r, \theta_w)/v_{r0}$ is the ratio of velocity at the wall ($v_r(r, \theta_w)$) to the centerline velocity (v_{r0}). F is, thus, a measure of the effective wall friction and varies in the range (0,1). $F = 0$ corresponds to perfect slip ($v_r(r, \theta_w) = v_{r0}$) and frictionless walls, as in the Savage [14] model. $F = 1$ corresponds to no slip at the wall ($v_r(r, \theta_w) = 0$). The data indicate that the centerline velocity (v_{r0}) varies inversely with radial distance (r) while the effective wall friction (F), increases linearly with r . Thus, the wall slip velocity normalized by the centerline velocity decreases with radial distance. The lines in Fig. 10b,c are fits of the following equations

$$v_{r0} = a_0/r + a_1, \quad F = b_0 + b_1 r. \quad (11)$$

Since a_1 and b_1 are both non-zero, this implies that the tangential velocity, v_θ , is non-zero from the continuity equation, assuming a constant bulk density.

Fig. 11 shows the variation of the tangential velocity (v_θ) with angle (θ) at different radial positions. The symbols are the measured values and the lines are predictions of v_θ obtained from the continuity equation using Eqs. (10) and (11), assuming a constant bulk density. The predictions are in good agreement with experimental data. The tangential velocity is about two orders of magnitude smaller than the radial velocity, v_r , in qualitative agreement with the model of Brennen and Pearce [15].

Fig. 12 shows the Beverloo [4] plot of the experimentally measured scaled mass flow rate ($(\dot{m}/\rho_p)^{2/3}/d_p$) versus the scaled orifice width (D_o/d_p) for $d_p = 1.86$ mm glass beads. The line is a fit to the data and yields $\alpha = 0.78$, which is significantly smaller than reported values. The lower value obtained is due to the presence of the front and back walls.

DEM simulations were carried out for a geometrically identical system as the experimental set up, including the front and back walls. All the walls are flat frictional surfaces. Period boundary conditions are used in the vertical direction (y -direction) so that particles exiting from the hopper are fed back at the top to maintain a constant fill height. The spring-dashpot model with friction was used,

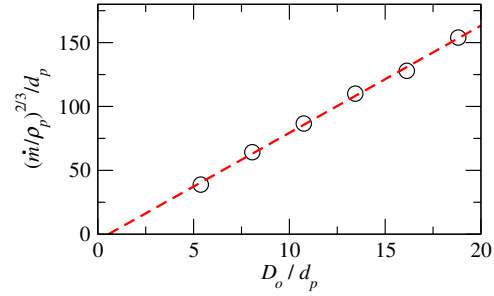


Figure 12. Beverloo plot for the scaled mass flow rate ($(\dot{m}/\rho_p)^{2/3}/d_p$) variation with the scaled orifice width (D_o/d_p). Symbols are experimental data for 1.86 mm glass beads and the line is a fit to the data.

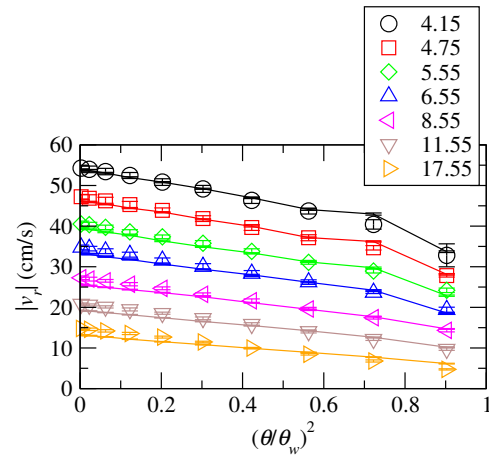


Figure 13. Experimental (symbols) and DEM simulation results (lines) for the variation of the velocity ($|v_r|$) with angle (θ) for $d_p = 1.86$ mm glass particles for orifice width $D_o = 2.5$ cm at different radial positions, r .

as above, with particle properties $d_p = 1.86 \pm 0.17$ mm, $\rho_p = 2.47$ g/cm³, $e = 0.9$ and $k_n = 5.686 \times 10^6$ dyn/cm. A number of simulations were carried out with the friction coefficients for particle-particle ($\mu_p \in (0.4, 0.6)$), particle-side wall ($\mu_w \in (0.4, 0.6)$) and particle-glass ($\mu_g \in (0.1, 0.2)$) contacts varied systematically over physically reasonable ranges for the parameters, as indicated. The set of friction coefficients that gave the best results are: $\mu_p = 0.5$, $\mu_w = 0.5$ and $\mu_g = 0.15$. A comparison of the simulation results for the velocity profile ($|v_r(r)|$), using the calibrated values of the friction coefficients (lines), with experimental measurements (symbols) is shown in Fig. 13. There is an excellent match between the two.

Fig. 14 shows simulation results for a similar system as in Fig. 10, but with the front and back walls removed and periodic boundary conditions applied in direction normal to the plane of the flow. The variation of the velocity ($|v_r|$) with the square of the scaled angle ($(\theta/\theta_w)^2$) for the simulated system without front and back walls is similar to that for the experimental quasi-2D system. The velocities are higher in the case of the simulations since the frictional resistance due to the front and back walls is absent. The variation of the centerline velocity (v_{r0}) with radial position is very similar to that of the simulation and ex-

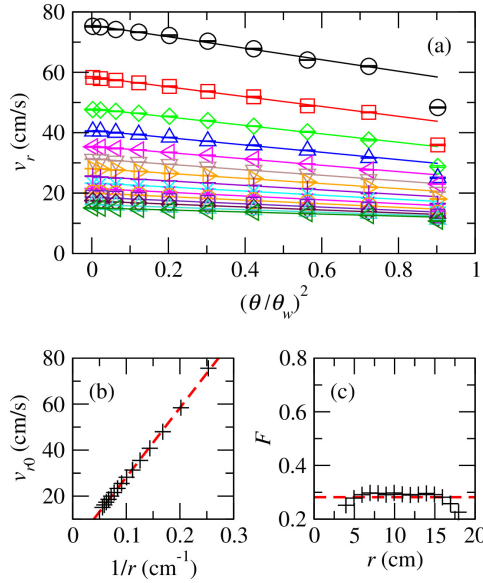


Figure 14. Simulation results for a system without front and back walls showing the variation of the radial velocity ($|v_r|$) with the square of the scaled angle $[(\theta/\theta_w)^2]$ for 1.86 mm glass particles orifice width $D_o = 2.5$ cm at different radial positions, r (symbols), as given in the legend of Fig. 10. Error bars indicate the standard error. Lines are fits of Eq. (10) to the data. (b) Variation of the fitted centerline velocity (v_{r0}) with $1/r$, and (c) fitted values of the effective wall friction (F) with radius (r). The lines in (b) and (c) are fits of Eq. (11) to the simulation data.

perimental results for the quasi-2D system. However, the effective friction (F) is nearly constant in the simulated system without the front and back walls in contrast to the linear increase with radial distance found for the quasi-2D system. The lower effective friction (F) for the system without front and back walls implies a higher relative slip velocity at the side walls.

The results presented above give a detailed experimental characterization of the velocity field in a quasi-2D hopper with front and back walls. DEM simulations indicate the velocity field is similar even in the absence of the walls. In the next section, we follow a similar approach and focus on the flow in the exit region, which is important for determining the flow rate from the hopper.

4 Flow in the exit region

We consider the flow in the exit region of the hopper by means of experiments and DEM simulations. The analysis is carried out in a region of dimensions $6\text{ cm} \times 6\text{ cm}$ centered on the exit plane as shown in Fig. 15, along with a definition of the coordinate system used. The experimental system and the simulation parameters are the same as described in the previous section. Results are reported for an orifice width, $D_o = 2.0$ cm and glass particles of diameter $d_p = 1.86 \pm 0.17$ cm. In addition to spatial distributions obtained by binning the data using square bins of side 0.1 cm, the variation along the centerline is considered by averaging using bins of height 0.1 cm and width $D_o/10$, in the region demarcated by dotted lines shown in Fig. 15.

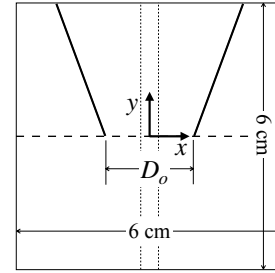


Figure 15. Schematic view showing the domain in the exit region used in the analysis. The coordinate system is defined. The horizontal dashed line shows the exit plane and the vertical dotted lines demarcate the region over which the centerline average is taken.

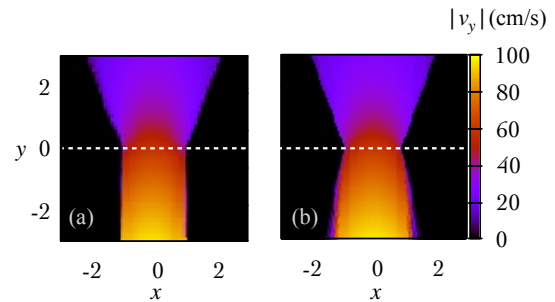


Figure 16. Spatial distribution of the vertical velocity $|v_y|$ for 1.86 mm glass beads in the exit region of a hopper with orifice width $D_o = 2.0$ cm. (a) Experimental measurements. (b) Simulation results.

Note that the region below the exit plane ($y < 0$) is also considered, unlike most previous studies.

Data in each experimental run are collected for 0.5 s after the flow reaches steady state, using the same method as described in the previous section. Each experiment is repeated 30 times and average values are reported along with the standard error. An identical protocol is followed in the DEM simulations. Such intensive averaging is necessary since we compute the acceleration, which requires a second derivative of the particle trajectory.

Fig. 16 shows the spatial distribution of the vertical velocity ($|v_y|$) for both experiments and simulations. There is a close match between the two. The velocity distributions vary smoothly for both, and there does not appear to be any surface at which a sharp change in velocity is evident.

Fig. 17 shows the variation of the vertical velocity and the scaled vertical acceleration along the centerline, for the experiments and DEM simulations. Simulation results for the system without the front and back walls are also shown in the figure. The DEM results for the system with front and back walls closely match the experimental results for the velocity and acceleration. The velocity variation with height is smooth and does not show any sharp changes (Fig. 17a), as found in the spatial distributions (Fig. 16). The scaled vertical acceleration, a_y/g , increases with decreasing height (y) until the magnitude becomes slightly greater than one ($a_y/g \approx 1.2$) inside the hopper near the exit plane ($y \approx 0.2$) and then decreases to $a_y/g = 1$ for heights below $y = -1$ cm (Fig. 17b). Thus, free fall of the

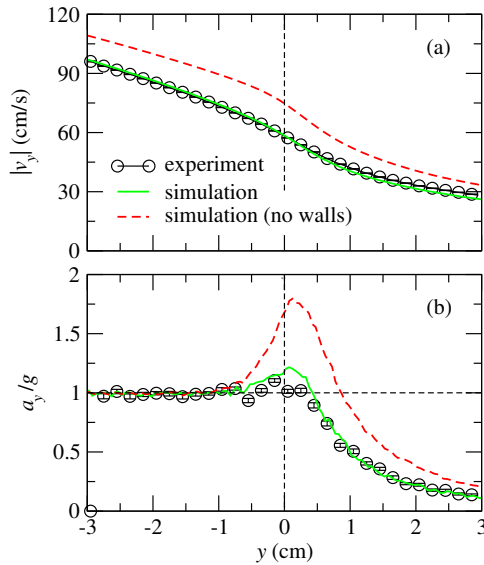


Figure 17. Variation of (a) the vertical velocity $|v_y|$, (b) the scaled vertical acceleration (a_y/g) with distance from the exit (y) for 1.86 mm glass beads in the exit region of a hopper with orifice width $D_o = 2.0$ cm. $y = 0$ (vertical dashed lines) corresponds to the position of the exit plane. Experimental data, DEM simulation results and DEM simulation results in the absence of the front and back walls are shown.

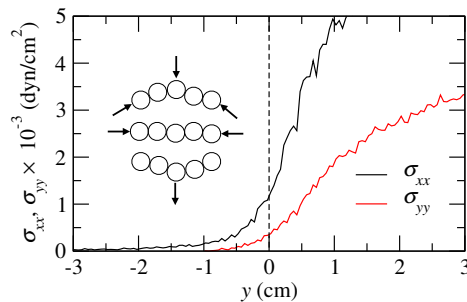


Figure 18. DEM simulation results for the variation of the normal stress components (σ_{xx} , σ_{yy}) with distance from the exit (y) for 1.86 mm glass beads in the exit region of a hopper with orifice width $D_o = 2.0$ cm. $y = 0$ (vertical dashed line) corresponds to the position of the exit plane. The steps of the mechanism of arch formation and buckling at the exit are shown schematically in the inset.

particles occurs only a significant distance below the exit plane.

The behaviour for the system without front and back walls (Fig. 17, dashed lines) is qualitatively similar to the quasi-2D system. The magnitude of the velocity is higher (Fig. 17a), which is expected. The magnitude of the acceleration peak is significantly larger ($a_y/g \approx 1.8$), which is unexpected from a physical view point.

The cause for the higher than g vertical acceleration (a_y) is related to the high magnitudes of the exit stresses, shown in Fig. 18, with the exit position marked by a dashed line. The stresses decrease with decreasing values of height (y) and horizontal stress (σ_{xx}) is significantly larger than the vertical stress (σ_{yy}). The higher values of the horizontal stress (σ_{xx}) are due to arch formation re-

sulting from the converging flow. The vertical stress compresses the arch, which eventually buckles downward. The buckling of the arch exerts a downward force, providing the impetus to the particles and increasing their acceleration. The steps of this mechanism – arch formation, compression and buckling – are shown schematically in the inset of Fig. 18. As a consequence of this mechanism, the stresses are non-zero below the exit plane ($y < 0$) with σ_{yy} going to zero at $y = -1$ cm and σ_{xx} going to zero at $y = -2$ cm.

5 Conclusions

We presented experimental and DEM simulation results related to flow in wedge-shaped hoppers.

DEM simulation results for a wedge-shaped hopper with frictionless walls are compared to the theoretical predictions of the Savage theory [14] and a theory based on the $\mu-I$ rheology. The simulation results show a significant exit stress, which is not accounted for in the Savage theory, and as a consequence the Savage theory predicts a higher flow rate than the simulation results. The $\mu-I$ model gives very good predictions of the velocity profile ($v_r(r)$), stress profile ($\sigma_{rr}(r)$) and stress ratio (k) using an empirical equation for the mass flow rate in place of a stress boundary condition at the exit. The inertia term in the momentum balance equation (Eq. 5) has a significant effect of the stress profile. The simulation results show large fluctuations, however, the time-averaged profiles match the profiles from theory. The mass flow rate from simulations follows the Beverloo correlation.

Experimental studies of the flow in a quasi-2D wedge-shaped hopper with front and back walls showed that the radial velocity in cylindrical coordinates varies as $v_r \propto \theta^2$. The flow is not purely radial, and we obtained a small tangential velocity. The results are in qualitative agreement with the theory of Brennen and Pearce [15]. Fits of an empirical equation to the data showed that the centerline velocity (v_{r0}) varies inversely with radial distance and the effective wall friction (F) increases linearly with radial distance. The latter implies that the wall slip velocity decreases with radial distance. The radial velocity from calibrated DEM simulations closely matches experimental results. DEM simulations for flow in the hopper with the calibrated parameters, but without front and back walls, gave similar results. The centerline velocity (v_{r0}) varies inversely with radial distance but the effective friction (F) is constant with radial distance and has a low value compared to the system with walls. Thus, the slip velocity in the system without front and back walls is higher than that for the system with walls.

Experiments and DEM simulations are carried out to analyze the flow in the exit region of the wedge-shaped hopper with front and back walls. The spatial velocity distributions and the velocity and acceleration variation along the centerline for the experiments and DEM simulations match closely. The results do not show any evidence of a sharp change in velocity, which would indicate the presence of a free fall arch. The vertical acceleration becomes

equal to the gravitational acceleration (free fall) significantly below the exit plane. The vertical acceleration is larger than the gravitational acceleration near the exit and an arch-buckling mechanism is proposed to explain the observation.

The results presented here suggest several avenues for further investigation. These include development of a theory and DEM simulations for hoppers with frictional walls, as well as building models for the flow in the exit region.

References

- [1] R.M. Nedderman, Statics and kinematics of granular materials (Cambridge University Press, 1992)
- [2] D. Schulze, Powders and Bulk Solids: Behavior, Characterization, Storage and Flow (Springer International Publishing, 2021)
- [3] R. Brown, J. Richards, Two-and three-dimensional flow of grains through apertures, *Nature* **182**, 600 (1958).
- [4] W.A. Beverloo, H.A. Leniger, J. Van de Velde, The flow of granular solids through orifices, *Chemical Engineering Science* **15**, 260 (1961).
- [5] A. Janda, I. Zuriguel, D. Maza, Flow rate of particles through apertures obtained from self-similar density and velocity profiles, *Physical review letters* **108**, 248001 (2012). <https://doi.org/10.1103/PhysRevLett.108.248001>
- [6] S.M. Rubio-Largo, A. Janda, D. Maza, I. Zuriguel, R. Hidalgo, Disentangling the free-fall arch paradox in silo discharge, *Physical Review Letters* **114**, 238002 (2015).
- [7] D. Gella, D. Maza, I. Zuriguel, Role of particle size in the kinematic properties of silo flow, *Physical Review E* **95**, 052904 (2017). <https://doi.org/10.1103/PhysRevE.95.052904>
- [8] R.L. Brown, J. Richards, Kinematics of the flow of dry powders and bulk solids, *Rheologica Acta* **4**, 153 (1965).
- [9] R. Nedderman, The measurement of the velocity profile in a granular material discharging from a conical hopper, *Chemical Engineering Science* **43**, 1507 (1988). [https://doi.org/10.1016/0009-2509\(88\)85142-X](https://doi.org/10.1016/0009-2509(88)85142-X)
- [10] J. Cleaver, R. Nedderman, Measurement of velocity profiles in conical hoppers, *Chemical Engineering Science* **48**, 3703 (1993). [https://doi.org/10.1016/0009-2509\(93\)81027-S](https://doi.org/10.1016/0009-2509(93)81027-S)
- [11] F. Vivanco, S. Rica, F. Melo, Dynamical arching in a two dimensional granular flow, *Granular Matter* **14**, 563 (2012). <https://doi.org/10.1007/s10035-012-0359-7>
- [12] A.W. Jenike, Steady gravity flow of frictional-cohesive solids in converging channels, *Journal of Applied Mechanics, Transactions ASME* **31**, 5 (1964). [10.1115/1.3629571](https://doi.org/10.1115/1.3629571)
- [13] A.W. Jenike, R. Shield, On the plastic flow of coulomb solids beyond original failure, *Journal of Applied Mechanics* **26**, 599 (1959).
- [14] S.B. Savage, The mass flow of granular materials derived from coupled velocity-stress fields, *British Journal of Applied Physics* **16**, 1885 (1965). [10.1088/0508-3443/16/12/313](https://doi.org/10.1088/0508-3443/16/12/313)
- [15] C. Brennen, J.C. Pearce, Granular material flow in two-dimensional hoppers, *Journal of Applied Mechanics* **46**, 529 (1978).
- [16] P. Jop, Y. Forterre, O. Pouliquen, A constitutive law for dense granular flows, *Nature* **441**, 727 (2006). [10.1038/nature04801](https://doi.org/10.1038/nature04801)
- [17] A.F. Momin, D.V. Khakhar, Granular flow in a wedge-shaped hopper with smooth walls and radial gravity: Theory and simulations, *Physical Review Fluids* **10**, 034303 (2025).
- [18] A.P. Thompson, H.M. Aktulga, R. Berger, D.S. Bolintineanu, W.M. Brown, P.S. Crozier, P.J. in 't Veld, A. Kohlmeyer, S.G. Moore, T.D. Nguyen et al., LAMMPS - a flexible simulation tool for particle-based materials modeling at the atomic, meso, and continuum scales, *Computer Physics Communications* **271**, 1 (2022). [10.1016/j.cpc.2021.108171](https://doi.org/10.1016/j.cpc.2021.108171)
- [19] S. Roy, S. Luding, T. Weinhart, A general(ized) local rheology for wet granular materials, *New Journal of Physics* **19**, 043014 (2017). [10.1088/1367-2630/aa6141](https://doi.org/10.1088/1367-2630/aa6141)
- [20] A. Bhateja, D.V. Khakhar, Analysis of granular rheology in a quasi-two-dimensional slow flow by means of discrete element method based simulations, *Physics of Fluids* **32**, 1 (2020). [10.1063/1.5123714](https://doi.org/10.1063/1.5123714)
- [21] D.G. Schaeffer, Instability in the evolution equations describing incompressible granular flow, *Journal of Differential Equations* **66**, 19 (1987).
- [22] T. Barker, D.G. Schaeffer, P. Bohórquez, J. Gray, Well-posed and ill-posed behaviour of the-rheology for granular flow, *Journal of Fluid Mechanics* **779**, 794 (2015).
- [23] J. Yogi, D.V. Khakhar, Granular flow in a quasi-2d wedge-shaped hopper: experiments and simulations, under review (2025).